DOI: 10.1002/chem.200901224

Reactivity and Regioselectivity of Noble Gas Endohedral Fullerenes $Ng@C_{60}$ and $Ng_2@C_{60}$ (Ng = He–Xe)

Sílvia Osuna,[a] Marcel Swart,*[a, b] and Miquel Solà*[a]

Abstract: Recently, it was shown that genuine Ng–Ng chemical bonds are present in the endohedral fullerenes $Ng_2@C_{60}$ in the case of Ng = Xe, while it is more debatable whether a chemical bond exist for Ng = Ar and Kr. The lighter homologues with helium and neon are weakly bonded van der Waals complexes. The presence of a noble gas dimer inside the cage is expected to modify the exohedral reactivity of the C_{60} cage with respect to that of free C_{60}. To investigate the impact of encapsulated diatomic noble gas molecules on the chemical reactivity of C_{60}, we analyzed the thermodynamics and the kinetics of [4+2] Diels–Alder cycloaddition of 1,3-*cis*-butadiene at all non-equivalent bonds in free C_{60}, $Ng@C_{60}$, and $Ng_2@C_{60}$ (Ng = He, Ne, Ar, Kr, and Xe). Our BP86/TZP calculations reveal that introduction of single noble gas atoms in $Ng@C_{60}$ and noble gas dimers He_2 and Ne_2 in $Ng_2@C_{60}$ has almost no effect on the exohedral reactivity compared to free C_{60}, in agreement with experimental results. In all these cases cycloaddition is clearly favored at the [6,6] bonds in the fullerene cage. For the endohedral compounds $He_2@C_{60}$ and $Ne_2@C_{60}$ a slight preference (by less than 2 kcal mol^{-1}) for bonds closer to the C_5 symmetry axis is found. This picture changes dramatically for the endohedral compounds with heavier noble gas dimers. Encapsulation of these noble gas dimers clearly enhances the reaction, both under thermodynamic and kinetic control. Moreover, in the case of $Xe_2@C_{60}$, addition to [6,6] and [5,6] bonds becomes equally viable. These reactivity changes in endohedral fullerenes are attributed to stabilization of the LUMO, increased fullerene strain energy, and greater compression of the encapsulated Ng_2 unit along the He to Xe series.

Keywords: cycloaddition · density functional calculations · fullerenes · noble gases · reaction mechanisms

Introduction

The possibility of encapsulating atoms or molecules inside fullerenes was considered after the first fullerene was discovered in 1985,[1] when Heath et al. synthesized the first endohedral compound $La@C_{60}$. Six years later, endohedral compounds with encapsulated noble gases were synthesized by collision of helium, neon, or argon atoms with C_{60}^+ or of noble gas cations with neutral C_{60}.[2] In 1993, Saunders and co-workers showed that, in fullerene preparation by the standard method (graphite arc in low-pressure helium), the endohedral compound $He@C_{60}$ was obtained for about one in a million free fullerene molecules.[3] Moreover, heating fullerenes to high temperatures under several atmospheres of ^{3}He or Ne produced the respective endohedral compounds. The presence of potassium cyanide in the reaction mixture enhances the rate of the reaction.[4] Using the same procedure, Saunders et al. discovered that all noble gas endohedral compounds could be produced under the same conditions.[3,5] The proposed formation mechanism is reversible breaking of a carbon–carbon bond of the fullerene surface, which opens a "window" large enough to allow noble gas encapsulation.[6] Jiménez-Vázquez et al. used classical statistical mechanics to estimate the equilibrium constants for encapsulation of noble gas atoms in C_{60}.[7] Since then, several studies on purification and enrichment of these compounds have been carried out.[8] A significant advance in the insertion of atoms and molecules into the C_{60} cage and production of macroscopic quantities of endohedral fullerenes

[a] S. Osuna, Dr. M. Swart, Prof. Dr. M. Solà
Institut de Química Computacional and Departament de Química
Universitat de Girona, Campus Montilivi, 17071 Girona (Spain)

[b] Dr. M. Swart
Institució Catalana de Recerca i Estudis Avançats (ICREA)
Pg. Lluís Companys 23, 08010 Barcelona (Spain)

Supporting information for this article is available on the WWW under http://dx.doi.org/10.1002/chem.200901224. It contains Cartesian coordinates of all species, including imaginary frequencies of the TSs, a figure showing the orientation of the noble gas dimer in the different products for Ng = He, Ne, Ar, and Xe, and HOMOs and LUMOs of the different $Ng_2@C_{60}$ species.

was made by Komatsu et al.[9] with chemical opening, insertion, and chemical closing of the cage in what has been called fullerene surgery. This process allowed the synthesis of $He@C_{60}$ and other endohedral fullerenes.[10,11] $^3He@C_{60}$ species are chemically interesting because ^3He NMR spectroscopy can be used to study reactions of fullerenes.[12,13] NMR studies on $^3He@C_{60}$ and $^3He@C_{70}$ indicate significant diamagnetic rings in C_{60} and very large ones in C_{70}.[14] Although $Ng@C_{60}$ (Ng = He–Xe) compounds have been theoretically studied in several works,[15,16] none of them analyzed their reactivity.

Interestingly, endohedral fullerenes with a single noble gas atom were detected in deposits associated with the impact of a large bolide (asteroid or comet) with the Earth (i.e., the Sudbury Impact Crater).[17] The Sudbury fullerenes (C_{60} and C_{70}) were found to contain anomalous ratios of $^3He/^4He$ indicating that the fullerene component is extraterrestrial in origin. Other endohedral fullerenes containing noble gases such as $^{40}Ar/^{36}Ar$ in nonterrestrial ratios were also found. Endohedral compounds with single noble gas atoms are stable, although the rate of decomposition to the free fullerene and noble gas is faster if traces of trapped solvent are not removed.[18]

Frunzi, Cross, and Saunders explored experimentally the exohedral reactivity of these single-Ng compounds. They performed the Diels–Alder reaction between 9,10-dimethylanthracene (DMA) and $^{129}Xe@C_{60}$ or $^3He@C_{60}$ to investigate the effect of the trapped noble gas.[19] They observed that the thermodynamics of the Diels–Alder reaction was favored at low temperatures in the case of $^3He@C_{60}$, while at high temperatures the equilibrium constant of the reaction was larger for $^{129}Xe@C_{60}$. Moreover, they obtained 85% of bis-adducts and no measurable amount of unreacted $^3He@C_{60}$ in the case of helium. When xenon is encapsulated inside, some unreacted $^{129}Xe@C_{60}$ and large amounts of mono-adduct were detected. According to Frunzi, Cross, and Saunders ,[19] the decreased reactivity of $^{129}Xe@C_{60}$ towards addition of DMA compared to $^3He@C_{60}$ at low temperatures must be attributed to the fact that the π-electron cloud of the C_{60} cage is pushed outward by the xenon atom. The same reason was given by Komatsu et al. to justify the decreased reactivity of $(H_2)_2@C_{70}$ compared to $H_2@C_{70}$.[11] Recently, Diels–Alder and retro-Diels–Alder reaction between DMA and $H_2@C_{60}$ was also studied.[20] The authors reported that the equilibrium constant for $H_2@C_{60}$ is the same as that of $^3He@C_{60}$.[20]

In 1997, Giblin and co-workers proposed that formation of endohedral fullerenes containing two noble gas atoms is possible,[21] and the first such noble gas endohedral compounds were obtained in 1998, when two helium or two neon atoms were encapsulated inside C_{70}.[22,23] In 2002, Sternfeld et al. introduced for the first time two helium atoms into C_{60}.[24] The ratio of $He@C_{60}$ to $He_2@C_{60}$ was 200:1, while it was 20:1 for the corresponding C_{70} compounds $He@C_{70}$ and $He_2@C_{70}$. $Ne_2@C_{60}$ may have also been observed in the experiment, although only $Ne_2@C_{70}$ and $HeNe@C_{70}$ could be definitively identified.[23]

The finding of two noble gas atoms close to each other was quite an achievement, since the attractive force between two noble gas atoms is small. Therefore, a free dimer of such atoms is only stable at extremely low temperatures or for a very short time in a collision. When these atoms are incorporated into the fullerene structure, they are forced into contact by the cage and vibrate and rotate within it like diatomic molecules. Moreover, the Ng–Ng distances in $Ng_2@C_{60}$ are much shorter than those in the free Ng_2, which are weakly bonded van der Waals complexes.[25]

The viability of dimer formation inside fullerenes has attracted interest. Scuseria and co-workers performed theoretical calculations on $Ng@C_{60}$ (Ng = He, Ne, Ar, Kr, and Xe) and $Ng_n@C_{60}$ (Ng = He, n = 2–4; Ng = Ne, n = 2).[16] In all cases studied they concluded that C_{60} was hardly deformed after encapsulation (less than 0.5 kcal mol^{-1} for a single noble gas atom, and 1 kcal mol^{-1} for multiple complexes at the B3LYP/6-31G**//LDA/3-21G level). The interaction energies for the systems considered were predicted to be repulsive: around 1 kcal mol^{-1} for $He@C_{60}$ and $Ne@C_{60}$, 7 and 14 kcal mol^{-1} for $Ar@C_{60}$ and $Kr@C_{60}$, and 7–30 kcal mol^{-1} for the $He_2@C_{60}$ and $He_4@C_{60}$ complexes. Note, however, that the level of theory used in their study is inadequate for weak interactions.[26] This was shown more explicitly by Lee and McKee for the interaction energy of one hydrogen molecule in a C_{60} fullerene ($H_2@C_{60}$), which was calculated as +1.7 kcal mol^{-1} with B3LYP and −6.5 kcal mol^{-1} at the more appropriate M05-2X level.[27]

Recently, Krapp and Frenking studied the chemical bonding of the noble gas atoms in the endohedral fullerenes $Ng_2@C_{60}$ (Ng = He, Ne, Ar, Kr and Xe).[25] The MP2/TZVPP//BP86/TZVPP calculations showed that equilibrium geometries for the considered compounds have D_{3d} symmetry with the exception of $Xe_2@C_{60}$, which was 2.8 kcal mol^{-1} more stable in the D_{5d} symmetry. Moreover, they observed that precession of the helium dimer in $He_2@C_{60}$ has practically no barrier. The charge distribution and orbital analysis showed that the partial charge of the Ng_2 dimer is close to zero, except for xenon. The sum of the atomic partial charges of the Xe_2 moiety is +1.06 and +1.52 for the lowest lying singlet and triplet states, respectively. Therefore between 1 and 2 electrons are transferred from the noble gas dimer to the fullerene structure, that is, $Xe_2^{q+}@C_{60}^{q-}$ ($1 < q < 2$). These results give clear evidence that a genuine chemical bond exists between xenon atoms. Less clear is the situation for Ar and Kr. $He_2@C_{60}$ and $Ne_2@C_{60}$ are theoretically predicted to have similar reactivity to the free fullerene C_{60}, as the carbon–carbon bond lengths were not severely modified upon encapsulation of the noble gas atoms, and charge transfer between noble gas atoms and the cage is close to zero. However, the C–C distances in the optimized structures of $Ar_2@C_{60}$, $Kr_2@C_{60}$, and especially $Xe_2@C_{60}$ are clearly elongated. The exohedral reactivity of these compounds is therefore expected to be different. The greater electron transfer in the case of the heaviest noble gas atoms reduces the electron affinity of the cage and thus should decrease the exohedral reactivity of the endohedral compounds on

going from Ng = He to Xe in $Ng_2@C_{60}$. In addition, the π-electron cloud of the C_{60} cage may be pushed outward by the heaviest noble gas atoms, and this also may reduce the chemical reactivity from He to Xe.[19] On the other hand, as pointed out by Krapp and Frenking,[25] the HOMO–LUMO gap is reduced and the strain grows from He to Xe, so an increase in exohedral reactivity of the C_{60} cage along the series He to Xe in $Ng_2@C_{60}$ could also be expected. Since these different effects counteract each other, it is unclear whether the chemical reactivity will increase or decrease when He is substituted by Xe in $Ng_2@C_{60}$ systems.

In recent years, interest in endohedral metallofullerenes (EMFs) has been growing due to their potential applications in medicine, biology, and nanotechnology.[28] A significant current topic is the exohedral reactivity of these compounds. Although functionalization and chemistry of free fullerene cages is quite well understood, far too little is known about the endohedral compounds. In several cases the endohedral cluster plays a major role in controlling the exohedral reactivity and regioselectivity of EMFs,[29] and detailed theoretical calculations are still needed to completely understand the exohedral reactivity of these compounds.[30,31] To the best of our knowledge, a theoretical study on the exohedral reactivity of these noble gas endohedral compounds has not been done before. Therefore, we studied the Diels–Alder reaction between 1,3-*cis*-butadiene and all nonequivalent bonds of noble gas endohedral compounds $Ng@C_{60}$ and $Ng_2@C_{60}$ (Ng = He, Ne, Ar, Kr, and Xe) with the aim of discussing the changes in reactivity and regioselectivity induced by the noble gas atoms on going from He to Xe. We studied both the thermodynamics and the kinetics for the compounds with encapsulated noble gas dimers, as thermodynamic and kinetic control do not always favor the same adduct in some related cases.[32] However, for encapsulation of single noble gas atoms, we only studied addition to the most reactive [6,6] bond in C_{60} thermodynamically and kinetically, while attack on the [5,6] bond was analyzed only from a thermodynamic point of view.

Computational Details

All DFT calculations were performed with the Amsterdam Density Functional (ADF) program.[33,34] The molecular orbitals were expanded in an uncontracted set of Slater-type orbitals (STOs) of triple-ζ (TZP) quality containing diffuse functions and one set of polarization functions.[35] To reduce the computation time, the frozen-core approximation was used.[34] This approximation is fundamentally different from using effective core potentials (ECPs). Although within the frozen-core approach in ADF core electrons are not included in the SCF procedure, it does include the core orbitals and explicitly orthogonalizes the valence orbitals to them. Therefore, in this work core electrons (1s for 2nd period, 1s2s2p for 3rd and 4th periods, 1s2s2p3s3p4s3d for 5th period) were not treated explicitly during the geometry optimizations (frozen-core approximation),[34] as this was shown to have a negligible effect on the obtained geometries and energetics.[36] Scalar relativistic corrections were included self-consistently by using the zeroth-order regular approximation (ZORA).[37] A previous study[38] on group 16 hydrides and halogen dimers already showed that the effect of the frozen core approach is small, and the relativistic effects only played a major role for the 5th period onwards.

An auxiliary set of s, p, d, f, and g STOs was used to fit the molecular density and to represent the Coulomb and exchange potentials accurately for each SCF cycle. Energies and gradients were calculated by using the local density approximation (Slater exchange and VWN correlation[39]) with nonlocal corrections for exchange (Becke88)[40] and correlation (Perdew86)[41] included self-consistently (i.e., the BP86 functional).

Although it is well documented that standard DFT functionals like BP86 underestimate energy barriers[42] (in the case of the parent Diels–Alder reaction between ethylene and 1,3-*cis*-butadiene BP86/TZP predicts a barrier of 18.6 kcal mol^{-1}, that is, an underestimation of the experimental value by some 6 kcal mol^{-1}), this underestimation should be similar for all Diels–Alder transition states (TSs) we encounter here and therefore should not affect the qualitative conclusions of the present study.[30]

The actual geometry optimizations and TS searches were performed with the QUILD[38,43] (QUantum regions Interconnected by Local Descriptions) program, which functions as a wrapper around the ADF program. The QUILD program constructs all input files for ADF, runs ADF, and collects all data; ADF is used only for generation of the energy and gradients. Furthermore, the QUILD program uses improved geometry optimization techniques, such as adapted delocalized coordinates[43] and specially constructed model Hessians with the appropriate number of eigenvalues.[43] The latter is of particular use for TS searches. All TSs were characterized by computing the analytical[44] vibrational frequencies, to have one (and only one) imaginary frequency corresponding to the approach of the two reacting carbon atoms (see Supporting Information for TS imaginary frequencies). In some cases, the located TSs had more than one imaginary frequency corresponding to rotation of the noble gas dimer. However, a full scan of these additional imaginary frequencies showed that they in fact have positive values and thus that the optimized structure is indeed a first-order saddle point (TS).

Pyramidalization angles, introduced by Haddon and Chow[45] as a measure of the local curvature in polycyclic aromatic hydrocarbons, were calculated with the POAV3 program.[46]

Results

Diels–Alder reactions of $Ng@C_{60}$ (Ng=He–Xe): To obtain reference values for the reaction energy and energy barrier, we studied the Diels–Alder reaction of free C_{60}, which has only two types of nonidentical bonds because of the high icosahedral (I_h) symmetry of the free fullerene cage: pyracylenic bonds at the junctions of two hexagonal rings ([6,6] bonds) and corannulenic bonds at the junctions between hexagonal and pentagonal rings ([5,6] bonds). The reaction at the [6,6] bonds of free C_{60} has a reaction energy of −20.7 kcal mol^{-1}, whereas at the [5,6] bonds the cycloaddition reaction is substantially less favorable (−4.6 kcal mol^{-1}). This result concurs with the experimental[47,48] and theoretical[49] evidence that the [6,6] bonds in C_{60} are more reactive in Diels–Alder reactions than the [5,6] bonds. In addition, the reaction energy found is close to the reaction enthalpies of −22.9 and −19.8 ± 2 kcal mol^{-1} obtained for Diels–Alder reaction of C_{60} with DMA[13] and cyclopentadiene,[50,51] respectively. The latter value was estimated from the enthalphy barriers of Diels–Alder[50] and retro-Diels–Alder[51] reactions between C_{60} and cyclopentadiene.

Then, we analyzed the Diels–Alder reaction at the two different nonequivalent bonds of the $Ng@C_{60}$ compounds (Ng = He-Xe). Since the exohedral reactivity of C_{60} occurs

mainly at the [6,6] bond,[47,49] for this bond we studied both thermodynamics and kinetics of addition, whereas we studied the Diels–Alder reaction at the [5,6] bond only from a thermodynamic point of view.

Table 1 lists reaction energies for different [6,6] and [5,6] additions to Ng@C_{60} (Ng = He–Xe). The reaction is substantially more favorable at [6,6] bonds than at [5,6] bonds (the energy difference is approximately 16 kcal mol^{-1} in all cases studied). The Diels–Alder reaction at the [6,6] bond of free C_{60} has a reaction energy of −20.7 kcal mol^{-1}, whereas in Ng@C_{60} it is −20.5, −20.3, −20.2, −20.3, and −20.5 kcal mol^{-1} for Ng = He, Ne, Ar, Kr, and Xe, respectively. Therefore, a decrease of the reaction energy is observed from He@C_{60} to Ar@C_{60}, while the opposite trend is observed for Kr@C_{60} and Xe@C_{60}, for which the reaction is slightly more favorable. The effect of substituting He by Xe in Ng@C_{60} is small, with energy differences of less than 0.1 kcal mol^{-1} according to our theoretical data. Experiments[19] also show small differences in reactivity, although slightly in favor of the He@C_{60} over Xe@C_{60}. In general, the computed reactivity differences are so small and below the average errors expected for these calculations that a clear trend cannot be derived, and one can only conclude that the reactivity of free C_{60} is almost unchanged by encapsulation of a single noble gas atom. The same tendencies are observed for the [5,6] bonds, as the reaction energy for free C_{60} is −4.6 kcal mol^{-1}, and in Ng@C_{60} they are −4.1, −3.9, −3.7, −3.9, and −4.1 kcal mol^{-1} along the series He@C_{60} > Ne@C_{60} > Ar@C_{60} < Kr@C_{60} < Xe@C_{60}. Therefore, the exohedral reactivity of the C_{60} cage is hardly affected by encapsulation of single noble gas atoms. Moreover, the optimized product corresponding to the addition of butadiene at the [6,6] bond of Ng@C_{60} is similar to that found for free C_{60} in all cases studied (the length of the C–C bonds that are formed in the reaction R_{cc} is 1.575 Å for both C_{60} and Ng@C_{60}). The final R_{cc} values of the different products for the addition to [5,6] bonds in Ng@C_{60} are approximately the same as those observed in C_{60} (R_{cc} is 1.572 Å for He–Ne@C_{60} and C_{60}, and 1.635 Å for Ar–Xe@C_{60}). We also calculated the activation barriers for the different noble gas endohedral compounds at the more reactive [6,6] bonds. The activation barrier for the [6,6] bond in free C_{60} is 12.7 kcal mol^{-1}, which is not far from the barriers obtained for Ng@C_{60}. The activation energy of the process increases slightly from He@C_{60} to Ar@C_{60} (13.0, 13.4, 13.3 kcal mol^{-1}, respectively). However, in similar fashion as for the reaction energies, the barrier decreases to 13.1 and 12.9 for the Kr@C_{60} and Xe@C_{60} compounds, respectively. At the transition state geometry, the length of the bonds that are being formed $R^{\neq}_{CC}$ is approximately the same as in C_{60} (the $R^{\neq}_{CC}$ values are 2.257 and 2.261 in free C_{60} and 2.259 Å in all Ng@C_{60} compounds). In the case of [5,6] bonds, we located the transition state only for the case of Kr, as these [5,6] bonds are much less reactive. The activation energy for the Diels–Alder reaction at the [5,6] bond in free C_{60} is 21.0 kcal mol^{-1}, which is 0.6 kcal mol^{-1} lower than that for Kr@C_{60} (21.6 kcal mol^{-1}). Therefore, encapsulation of a single noble gas inside the cage does not substantially affect the exohedral reactivity of C_{60}, as the reaction and activation energies as well as reactivity patterns are approximately the same.

Table 1. Reaction energies ΔE_R and activation energies $\Delta E^{\neq}$ [kcal mol^{-1}] corresponding to the addition of 1,3-*cis*-butadiene to [6,6] and [5,6] bonds of Ng@C_{60} (Ng = He–Xe).[a–c]

Ng@C_{60}	[6,6] bond		[5,6] bond
	ΔE_R	$\Delta E^{\neq}$	ΔE_R
He	−20.5	13.0	−4.1
Ne	−20.3	13.4	−3.9
Ar	−20.2	13.3	−3.7
Kr	−20.3	13.1	−3.9[c]
Xe	−20.5	12.9	−4.1

[a] Reaction energies for free C_{60} are −20.7 and −4.6 kcal mol^{-1} for the [6,6] and [5,6] bonds, respectively. [b] Activation energies for free C_{60} are 12.7 and 21.0 kcal mol^{-1} for the [6,6] and [5,6] bonds, respectively. [c] The activation barrier for the [5,6] bond of Kr@C_{60} is 21.6 kcal mol^{-1}.

Reaction energies for Diels–Alder reactions of Ng_2@C_{60} (Ng=He–Xe): The Diels–Alder reaction was studied at all nonequivalent bonds of the noble gas endohedral fullerenes (see Figure 1). Krapp and Frenking studied cage isomerism for noble-gas endohedral C_{60} compounds,[25] and found small differences in energy between the possible isomers D_{3d}, D_{5d}, and D_{2h}. The most stable was D_{3d} for all noble gases except for xenon, for which the D_{5d} isomer was more favorable. The same isomer should be considered in our study for all cases, so that the reactivities observed can be directly compared. We chose to study the D_{5d} isomer for a number of reasons. First, the most interesting noble gas endohedral fullerene is Xe_2@C_{60}, as a genuine chemical bond between the two xenon atoms is formed by transfer of one or two electrons to the fullerene cage (see Introduction). Second, encapsulation of helium, neon, argon, and krypton inside the D_{5d} cage gave structures that were less than 2 kcal mol^{-1} (SCS-MP2/TZVPP//BP86/TZVPP) less stable than for the D_{3d} isomer. Finally, in most cases the initial position of the

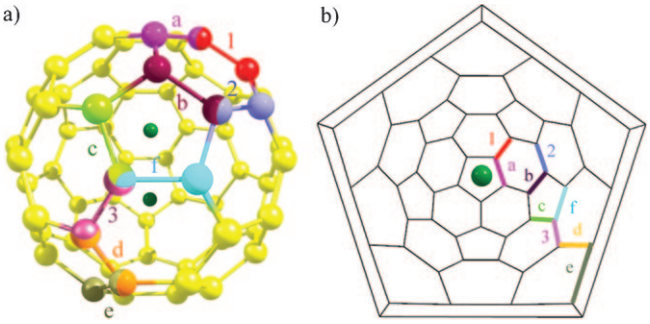

Figure 1. Nonequivalent bonds of Ng_2@C_{60} represented by different colors. All considered bonds are marked on the 3D structure of C_{60} (a) and on the Schlegel diagram (b), which converts the 3D structure to a 2D representation. The positions of the noble gas atoms are marked with green dots.

Table 2. Reaction energies ΔE_R [kcal mol^{-1}] and lengths [Å] of the C–C bonds at which the reaction took place (R_{full}) and for the bonds formed in the final products (R_{CC}).[a,b]

Bond	Bond type		$He_2@C_{60}$			$Ne_2@C_{60}$			$Ar_2@C_{60}$			$Kr_2@C_{60}$			$Xe_2@C_{60}$		
			ΔE_R	R_{full}	R_{CC}	ΔE_R	R_{full}	R_{CC}	ΔE_R	R_{full}	R_{CC}	ΔE_R	R_{full}	R_{CC}	ΔE_R	R_{full}	R_{CC}
		[6,6]	**−20.9**	1.610	1.572	**−23.1**	1.616	1.574	**−32.2**	1.644	1.567	**−39.9**	1.660	1.563	**−44.9**	1.676	1.554/1.561
		[6,6]	**−20.4**	1.605	1.575	**−23.1**	1.616	1.574	**−32.1**	1.644	1.567	**−39.9**	1.660	1.563	−43.3	1.680	1.559
		[6,6]	**−20.4**	1.608	1.575	**−21.1**	1.614	1.575	−21.4	1.636	1.575	−22.4	1.650	1.575	−22.3	1.645	1.574/1.576
a	D	[5,6]	−4.4	1.636	1.572	−6.4	1.641	1.572	−15.3	1.661	1.567	−24.1	1.671	1.560	**−44.6**	1.682	1.552
b	D	[5,6]	−4.2	1.636	1.572	−4.8	1.639	1.572	−15.3	1.661	1.567	−24.1	1.671	1.560	**−44.5**	1.682	1.552
c	D	[5,6]	−5.0	1.638	1.571	−5.0	1.641	1.570	−6.6	1.654	1.570	−7.1	1.664	1.570	−16.6	1.670	1.564/1.567
d	D	[5,6]	−4.2	1.636	1.572	−4.8	1.639	1.572	−6.0	1.652	1.572	−6.5	1.662	1.571	−15.7	1.669	1.568/1.565
e	D	[5,6]	−4.9	1.638	1.571	−5.3	1.641	1.570	−15.9	1.662	1.565	−24.7	1.673	1.558	**−45.5**	1.682	1.550
f	D	[5,6]	−4.9	1.638	1.571	−5.2	1.641	1.570	−2.3	1.613	1.574	−1.3	1.608	1.574	−9.5	1.606	1.571

[a] Reaction energies for free C_{60} are −20.7 and −4.6 kcal mol^{-1} for the [6,6] and [5,6] bonds, respectively. [b] In boldface: bonds that are most reactive under thermodynamic control.

noble gas dimer (and symmetry in general) is not preserved during the reaction, and in the final adducts the noble gas moiety usually faces the attacked bond (see below). With D_{5d} symmetry for $Ng_2@C_{60}$, six nonequivalent corannulene or type D [5,6] bonds **a–f** and three pyracylene or type A [6,6] bonds **1–3**) must be studied to take into account all possible additions (see Figure 1 and Table 2).

Table 2 and Figure 2 show the reaction energies for the different bonds of the noble gas endohedral fullerenes. The observed reaction energies of the helium compound are very close to those obtained for free C_{60}, and the most favorable addition sites are at all nonequivalent [6,6] bonds (−20.9, −20.4, and −20.4 kcal mol^{-1} for **1**, **2**, and **3**, respectively). All additions to [6,6] bonds show approximately the same reaction energies, but the geometry of the final adducts is significantly different. For example, Figure 3 shows the different Ng dimer orientations that were obtained in the final adducts for $Kr_2@C_{60}$ during the optimization process starting from the same initial $Ng_2@C_{60}$ D_{5d} geometry and just placing the 1,3-butadiene fragment at the corresponding bond. The geometries of the final adducts of the other $Ng_2@C_{60}$ (Ng = He, Ne, Ar, and Xe) endohedral compounds are included in the Supporting Information. Note that the final optimized adducts in each case are not, in general, the most stable conformer, which can be obtained by rotating the Ng_2 moiety and placing the Ng_2 fragment in front of the attacked bond.

In the case of bond **1**, during the optimization process, the encapsulated helium dimer has rotated from its initial position to a different configuration facing the bond that is being attacked by the butadiene. Although the noble gas dimer has not reoriented in cases **2** and **3**, the reaction energies corresponding to addition to these bonds are only 0.5 kcal mol^{-1} different from that obtained for bond **1**. The same holds for the [5,6] bonds, as the noble gas dimer has only rotated in the case of addition to bond **a**, and all obtained reaction energies are approximately −5.0 kcal mol^{-1}. Therefore, the exohedral reactivity of the endohedral compound is hardly affected by rotation of the helium dimer.

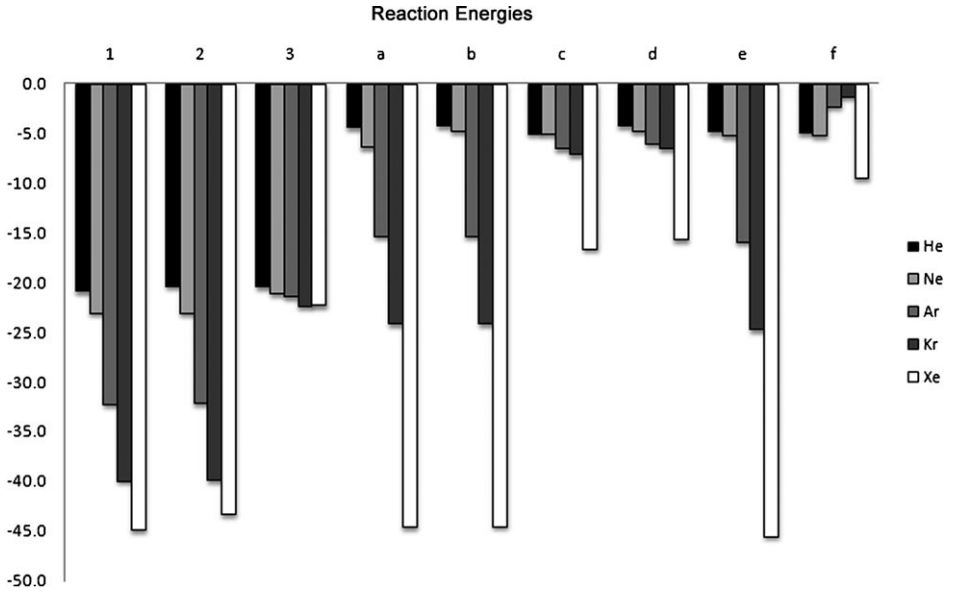

Figure 2. Comparison between the reaction energies [kcal mol^{-1}] for the Diels–Alder reaction over the nonequivalent bonds of the different endohedral fullerenes $Ng_2@C_{60}$.

To study the effect of dimer rotation more clearly, we performed an energy-surface scan for rotation of the noble gas dimers in the $Ng_2@C_{60}$ reactant. Figure 4 shows the energy profile corresponding to the rotational barriers for helium, neon, argon, and krypton. All points were calculated by single-point (SP) calculations at the optimized geometry of the reactant in which the noble gas dimer has been rotated from 0 to 90° with respect to the C_5 axis. The rotation energy barrier increases in the order He < Ne < Ar < Kr. The profile of Xe is not included in Figure 4, because in this case, unlike the other four noble gases, we did not obtain a

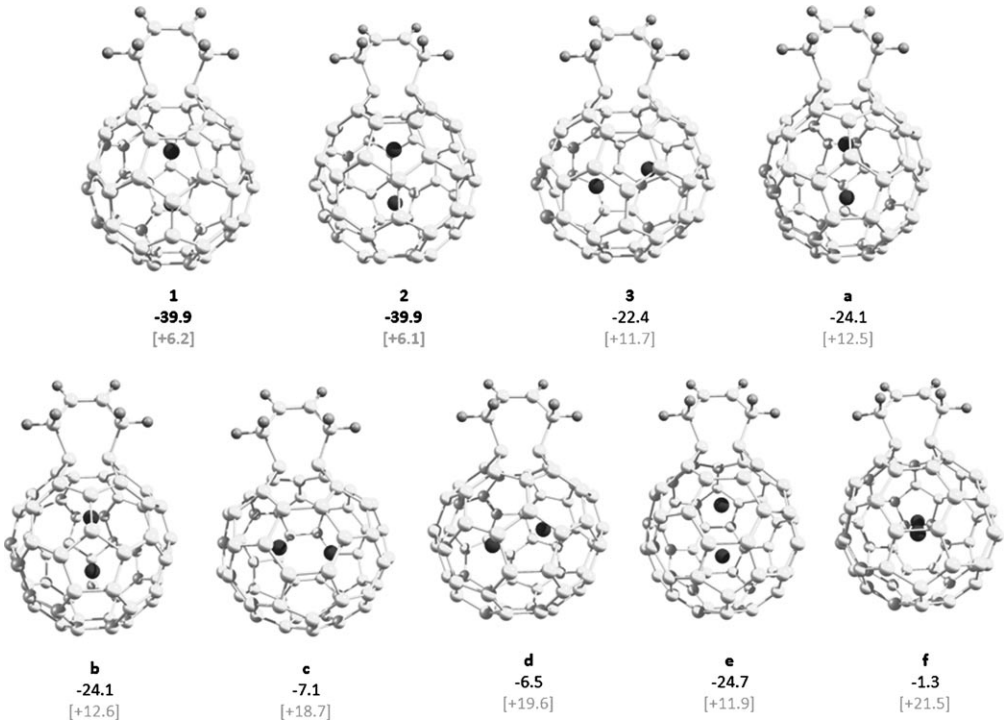

Figure 3. Optimized structures at the BP86/TZP level for the final adducts corresponding to the Diels–Alder reaction at all nonequivalent bonds of the endohedral compound $Kr_2@C_{60}$. Reaction energies [activation barriers] are also given. The most favorable addition sites are marked in boldface. Energies are given in kcal mol^{-1}.

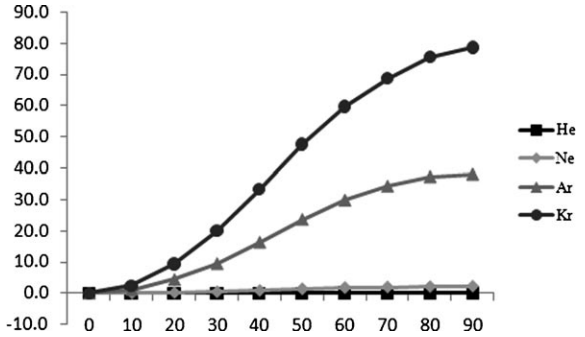

Figure 4. Rotational barriers for noble gas dimers inside C_{60}. The different points were obtained by performing several single-point calculations for rotation of the noble gas dimer from 0 to 90°. All energies are given in kcal mol^{-1}.

smooth energy profile. Probably, such a profile could be obtained by reoptimizing the geometry of $Xe_2@C_{60}$ for each fixed angle of rotation. Since the aim of Figure 4 is just to give a qualitative idea of the different rotational barriers for the different noble gas dimers, we considered it unnecessary to perform these time-consuming optimizations. Moreover, in the TS and product structures of $Ng_2@C_{60}$ the dimers were not constrained and might have reoriented, if energetically feasible.

Therefore, although these SP rotational energies are higher than might have been obtained through constrained-geometry optimizations, a qualitative interpretation of rotation of the noble gas dimer is still possible. As pointed out in previous quantum-chemical calculations and experimental NMR studies, helium atoms in $He_2@C_{60}$ move freely in the cage (practically no barrier is observed).[16,52] Rotation of the neon dimer is still possible, as the highest point on our energy surface lies below 2 kcal mol^{-1}. However, when larger noble gases are encapsulated, free rotation of the unit is no longer possible. The rotational barrier is less than 10 kcal mol^{-1} when the noble gas dimer is rotated from 0 to 30° for the argon dimer, and to 20° for the krypton dimer. These high barriers obtained for Ar and Kr are consistent with the large cage strain induced after encapsulation of large noble gas dimers inside the small C_{60} cavity (see Discussion). The C_{60} cage in Ar–Xe@C_{60} is extremely deformed and rotation of the Ng dimer is highly constrained. Hindered rotation of the encapsulated cluster due to the size of the cage has also been observed in other endohedral compounds $Sc_3N@C_x$, whereby Sc_3N encapsulated inside C_{80} can freely rotate, whereas it is highly constrained inside the smaller C_{78} cage.[53] Although the rotation of the xenon dimer is not included in Figure 4, its rotational barrier is expected to be higher than that of krypton.

The reaction energies for the neon-dimer endohedral compound are also close to those of the free compound. Bonds **1** and **2** have the most exothermic reaction energies (−23.1 kcal mol^{-1}), whereas bond **3** is slightly less reactive (−21.1 kcal mol^{-1}). Note that, although bonds **1** and **2** were initially inequivalent, after the reaction and rotation of the neon dimer the final adducts have exactly the same geome-

try and energy. The lower reactivity found for bond **3** is due to the absence of neon-dimer rotation. For bonds **1** and **2** the dimer has reoriented to a situation where it is facing the attacked bonds in the most favorable final adducts; however, this rotation does not occur for addition to bond **3**. This difference might be attributed to the positions of the different bonds. Rotation of the neon dimer from its initial position to facing bonds **1** and **2** is easier than for the case of bond **3** for different reasons (see Figure 1). First, rotation of the neon dimer from the initial position to face bond **3** requires a slightly higher rotational energy of approximately 2 kcal mol^{-1}. This could be easily surmounted, but rotation of the noble gas dimer occurs during addition of the butadiene, in the course of which the fullerene cage is distorted to accommodate pyramidalization of the carbon atoms involved in the reaction. Since the sum of all pyramidalization angles remains approximately constant during the cycloaddition process, parts of the C_{60} cage become somewhat flattened, and rotation of the noble gas dimer may be hindered to some extent by this geometrical distortion. Finally, for symmetry reasons (rotational gradients can be cancelled) rotation is more unlikely during the optimization process in bonds like **f** or those that are close to it (**3**, **c**, and **d**).

Cycloaddition to [5,6] bond **a** is somewhat more favorable than for the rest of the [5,6] bonds (the difference is 1.1–1.6 kcal mol^{-1}) due to neon-dimer rotation. However, the reactivity of [5,6] bonds is significantly lower, with reaction energies that range from −4.8 to −6.4 kcal mol^{-1}. The different orientations of the neon dimer hardly affect the reaction energies obtained, as cases in which the noble gas dimer has rotated have only slightly more favorable reaction energies, with differences of less than 2 kcal mol^{-1}.

The Diels–Alder reaction becomes more exothermic when larger noble gases are encapsulated inside the fullerene; on going to argon, krypton, and xenon the reaction energies increase to between −32.2 and −45.5 kcal mol^{-1}. In the case of argon, the preferred addition sites are again **1** and **2** (−32.2 and −32.1 kcal mol^{-1}, respectively), and the reaction at bond **3** is approximately 10 kcal mol^{-1} less favorable (−21.4 kcal mol^{-1}). Similar to the case for neon, argon-dimer rotation does not occur in the case of bond **3**. The difficulty of rotation when addition occurs at bonds situated in central positions affects the exohedral reactivity of the cage. The larger the encapsulated noble gas atoms, the more difficult is rotation from the initial position to the new orientation in which the dimer faces the attacked bonds (see Figure 1). The most favorable addition sites are over bonds close to the C_5 axis where the noble gas dimer is initially contained. The unreactive [5,6] bonds in the cases of helium and neon have considerably exothermic reaction energies for the heaviest members of the series (**a**, **b**, and **e** with reaction energies of approximately −16 kcal mol^{-1}). In those cases, the argon dimer has rotated and faces the bond involved in the reaction. This leads to substantially more exothermic reaction energies. The rest of the [5,6] bonds (**c**, **d**, and **f**), for which the noble gas dimer practically remains in the initial position, have reaction energies similar to those obtained for $He_2@C_{60}$ and $Ne_2@C_{60}$ (approximately −6 kcal mol^{-1} for **c** and **d**, and −2.3 kcal mol^{-1} for **f**). It seems reasonable to conclude that the higher exothermicity of bonds **1**, **2**, **a**, and **b** in the case of Ar and Kr is due to partial release of the destabilizing two-center four-electron interaction that occurs when the Ng–Ng distance increases from its initial value to that which it has in the adduct, because the final product has more space to accommodate the dimer. In the case of xenon, transfer of 1–2 electrons from the Ng dimer to the fullerene cage takes place (total charge of XeXe at the BP86/TZP level is +1.20 e and is practically unchanged during reaction). Although in the latter case there is a stabilizing two-center three-electron interaction, the Xe–Xe distance is slightly increased after reaction. This is mainly attributed to the fact that Xe_2 is highly compressed inside C_{60} (the Xe–Xe distance inside the fullerene for adduct **1** is 2.557 Å, whereas the optimized BP86/TZP distance for free $[XeXe]^+$ is 3.372 Å).

Like for the other noble gas endohedral compounds, the preferred addition sites for $Kr_2@C_{60}$ are [6,6] bonds **1** and **2** (the reaction energy is −39.9 kcal mol^{-1}). The other [6,6] bond **3** is approximately 18 kcal mol^{-1} less reactive (the reaction energy is −22.4 kcal mol^{-1}) than **1** and **2**, even though it also has a short C–C distance (Table 3). Moreover, it is now even less favorable than some of the [5,6] bonds. Indeed, the [5,6] bonds for which rotation of the noble gas dimer has taken place (**a**, **b**, and **e**) have reaction energies of about −24 kcal mol^{-1}. Nevertheless, the difference in reactivity between the most reactive [6,6] and most reactive [5,6] bonds

Table 3. Bond lengths R_{CC} [Å] and pyramidalization angles θ_p [°] for the bond types in free and endohedral fullerenes.[a]

Bond	Bond type		$He_2@C_{60}$		$Ne_2@C_{60}$		$Ar_2@C_{60}$		$Kr_2@C_{60}$		$Xe_2@C_{60}$	
			R_{CC}	θ_p[b]	R_{CC}	θ_p[b]	R_{CC}	θ_p[b]	R_{CC}	θ_p[b]	R_{CC}	θ_p[b]
		[6,6]	1.400	11.67	1.403	11.75	1.418	12.08	1.427	12.30	1.432	12.63
		[6,6]	1.398	11.63	1.397	11.60	1.394	11.51	1.395	11.45	1.401	11.16
		[6,6]	1.398	11.62	1.399	11.57	1.403	11.32	1.406	11.14	1.422	11.90
a	D	[5,6]	1.454	11.73	1.459	11.94	1.475	12.63	1.489	12.85	1.502	12.51
b	D	[5,6]	1.454	11.62	1.455	11.58	1.460	11.52	1.466	11.60	1.472	11.95
c	D	[5,6]	1.454	11.63	1.456	11.59	1.462	11.42	1.466	11.30	1.470	11.53
d	D	[5,6]	1.454	11.63	1.456	11.59	1.462	11.42	1.466	11.29	1.470	11.53
e	D	[5,6]	1.454	11.62	1.455	11.59	1.460	11.52	1.466	11.60	1.472	11.96
f	D	[5,6]	1.452	11.62	1.450	11.57	1.443	11.32	1.440	11.14	1.430	11.90

[a] For comparison, the [6,6] and [5,6] distances in free C_{60} at the BP86/TZP level are 1.398 and 1.453 Å, and $\theta_p = 11.64°$. [b] Pyramidalization angles averaged over both atoms that constitute the bond under consideration.

is still quite large (ca. 16 kcal mol^{-1}). The other [5,6] bonds have reaction energies that range from −1.3 (**f**) to about −7.0 kcal mol^{-1} (**c** and **d**). This difference of 6 kcal mol^{-1} is mainly attributed to the degree of rotation of the noble gas dimer. In the case of bond **f** the krypton dimer remains in the initial position, whereas in the cases of bonds **c** and **d** it is slightly rotated to a more favorable situation.

Interesting results were obtained for $Xe_2@C_{60}$. Krapp and Frenking observed that the sum of atomic charges of the Xe_2 moiety is +1.06 at the BP86/TZVPP level in the lowest-lying singlet state, that is, about one electron is transferred from the noble gas dimer to the fullerene cage ($Xe_2^+@C_{60}^-$).[25] This clearly indicates that a chemical bond between xenon atoms is formed. Moreover, they expected a profound change in the exohedral reactivity of the endohedral fullerene compared to the free cage, due to the structural variations of C_{60} after xenon-dimer encapsulation. Encapsulation of such large noble gas atoms inside the fullerene cage leads to elongation of all C–C bonds of the structure, except for bond **f**. However, [6,6] bonds still show the shortest bond lengths (1.401–1.432 Å, see Table 3).

The Diels–Alder reaction at the most favorable addition sites of $Xe_2@C_{60}$ gives five different cycloadducts. Reactions at bonds **1, 2, a**, **b**, and **e** have reaction energies of approximately −44.5 kcal mol^{-1}. Interestingly, cycloaddition is no longer regioselective, as [6,6] and [5,6] bonds are equally reactive. All reactive bonds are situated close to the C_5 axis, as rotation of the xenon dimer is highly impeded. Bond **a** has an extremely large C–C bond length in the initial reactant (1.502 Å), but addition here is extremely favorable. As we pointed out previously, introduction of large species inside fullerene cages leads to highly strained systems in which even unusually long [5,6] bonds can exhibit the most favorable reaction energies.[31] The rest of the considered bonds (**3, c**, **d**, and **f**) have less favorable reaction energies due to their central location and highly impeded rotation of Xe_2 inside the cage.

Activation barriers for the Diels–Alder reactions of $Ng_2@C_{60}$ (Ng=He–Xe): Energy barriers for the Diels–Alder reaction at all nonequivalent bonds and for all endohedral compounds were determined. The TS search always started from a symmetric structure, but an asynchronous TS structure was located after the optimization procedure in all cases.[54] The activation barriers for free C_{60} show the same trend as for the reaction energies, in that the reaction over [6,6] bonds is clearly favored (the barrier is 12.7 kcal mol^{-1}) compared to [5,6] bonds (barrier 21.0 kcal mol^{-1}). Again this is in agreement with experimental[47,48] and theoretical[49] evidence that the [6,6] bonds in C_{60} are more reactive in Diels–Alder reactions than the [5,6] bonds. The energy barrier obtained is not far from the experimental values of 14.1 and 6.9 kcal mol^{-1} obtained for the activation energies of the Diels–Alder reaction of C_{60} with anthracene[55] and cyclopentadiene,[50] respectively. Table 4 and Figure 5 show the activation barriers obtained for all noble gas endohedral compounds studied.

The preferred addition site for helium-dimer endohedral compounds under thermodynamic control was found to be [6,6] bond **1** (see above), which has a reaction energy similar to that of free C_{60}. Addition to this bond also has the lowest activation barrier (12.8 kcal mol^{-1}), which is again very close to the value observed for the free C_{60}. Bonds **2** and **3** have slightly higher activation barriers (13.1 kcal mol^{-1}), while the [5,6] bonds have reaction barriers that range from 20.4 to 21.5 kcal mol^{-1}. Therefore, for both [6,6] and [5,6] bonds we obtain values that are close to those of free C_{60}.

The same trends are observed for $Ne_2@C_{60}$. The preferred addition sites under thermodynamic control (bonds **1** and **2**) also have the lowest activation barriers (11.9 kcal mol^{-1}). Similar to the helium compound there is no significant change in the activation barriers compared to free C_{60}. The reaction at bond **3** is kinetically slightly less favored, with a reaction barrier that is 1.1 kcal mol^{-1} higher (13.0 kcal mol^{-1}). The addition to [5,6] bonds is much less favored, with activation barriers that are approximately 20 kcal mol^{-1} in all cases.

The Diels–Alder reaction to bonds **1** and **2** has a reaction barrier of 8.4 kcal mol^{-1} in the case of $Ar_2@C_{60}$. The activation barrier for the reaction at bond **3** is approximately 3 kcal mol^{-1} higher in energy than those for bonds **1** and **2**. Like in cases of the other noble gases, the activation energies corresponding to addition to [5,6] bonds are significantly higher. The barriers for those [5,6] bonds for which the noble gas dimer has rotated (**a**, **b**, and **e**) are about

Table 4. Activation energies $\Delta E^{\neq}$ [kcal mol^{-1}] and lengths R_{CC} [Å] of the C–C bonds that will be finally bound.[a,b]

Bond	Bond type		$He_2@C_{60}$		$Ne_2@C_{60}$		$Ar_2@C_{60}$		$Kr_2@C_{60}$		$Xe_2@C_{60}$	
			$\Delta E^{\neq}$	R_{CC}	$\Delta E^{\neq}$	R_{CC}	$\Delta E^{\neq}$	R_{CC}	$\Delta E^{\neq}$	R_{CC}	$\Delta E^{\neq}$	R_{CC}
		[6,6]	**12.8**	2.274/2.250	**11.9**	2.278/2.270	**8.4**	2.366/2.388	**6.2**	2.404/2.403	**4.9**	2.193/2.569
		[6,6]	**13.1**	2.210/2.311	**11.8**	2.290/2.255	**8.5**	2.336/2.336	**6.1**	2.402/2.402	**3.8**	3.065/2.140
		[6,6]	**13.1**	2.268/2.252	**13.0**	2.259/2.265	12.2	2.137/2.419	11.7	2.137/2.426	11.3	2.144/2.411
a	D	[5,6]	21.4	2.595/1.702	20.2	2.623/1.702	15.6	3.049/1.850	12.5	3.315/1.952	5.7	3.511/2.122
b	D	[5,6]	21.5	1.699/2.589	21.3	1.695/2.594	15.7	1.700/2.836	12.6	1.948/3.311	5.6	2.119/3.505
c	D	[5,6]	20.4	1.704/2.578	20.0	1.702/2.581	19.2	1.700/2.595	18.7	1.695/2.600	14.7	1.898/3.152
d	D	[5,6]	21.5	2.590/1.699	21.4	2.591/1.698	20.1	2.605/1.690	19.6	2.598/1.682	8.1	2.052/3.561
e	D	[5,6]	20.4	2.576/1.705	20.0	2.585/1.705	14.9	1.710/2.853	11.9	1.961/3.240	6.1	2.125/3.242
f	D	[5,6]	20.4	2.577/1.705	20.1	2.593/1.703	19.4	2.558/1.693	21.5	2.524/1.696	16.4	3.229/1.893

[a] Activation energies for free C_{60} are 12.7 and 21.0 kcal mol^{-1} for the [6,6] and [5,6] bonds, respectively. [b] In boldface: the bonds that are most reactive under kinetic control.

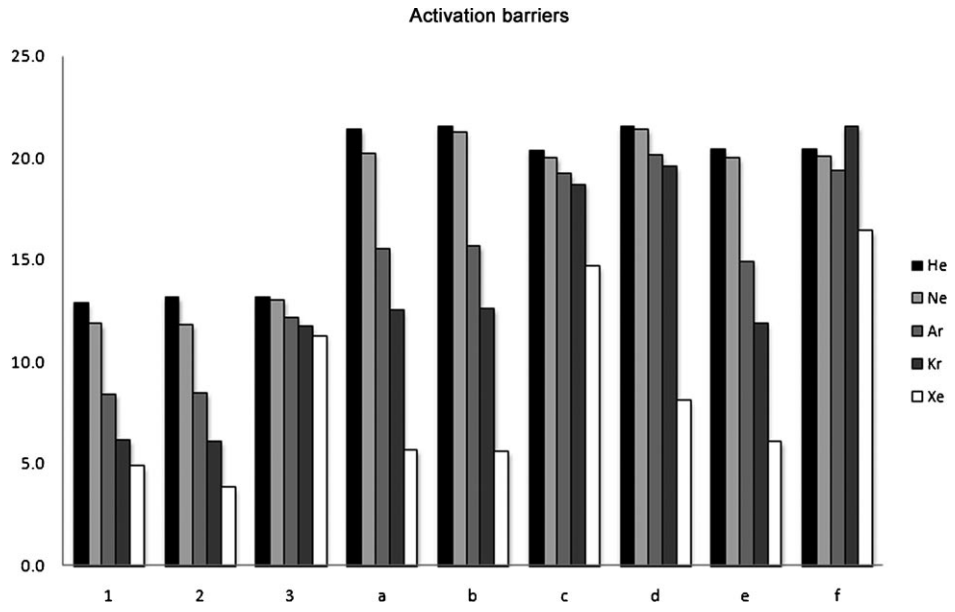

Figure 5. Comparison between activation barriers [kcal mol^{-1}] found for the Diels–Alder reaction at the nonequivalent bonds of the different endohedral fullerenes $Ng_2@C_{60}$.

15 kcal mol^{-1}, whereas for the others (**c**, **d**, and **f**) they are close to 20 kcal mol^{-1}.

The same tendencies are observed for krypton, but the activation barriers are approximately 2 kcal mol^{-1} lower than for argon. As was observed in the other compounds, the lowest activation energy is obtained for addition to bonds **1** and **2** (ca. 6 kcal mol^{-1}). Addition to the other [6,6] bond **3** is significantly less favorable with a barrier of about 12 kcal mol^{-1}, which is very close to those observed for some of the [5,6] bonds (**a**, **b**, and **e**). This pattern of almost equal reactivity for bonds **3**, **a**, **b**, and **e** also emerged for the reaction energies (see above). The most reactive [5,6] bonds in $Xe_2@C_{60}$ are those having the longest C–C bond length (1.47–1.49 Å). In $Y_3N@D_{3h}$-C_{78} the longest [5,6] bond (C–C 1.47 Å) is also the most reactive.[31]

Figure 6 shows the reactant, transition state, and product for addition to bonds **1** and **3** in $Kr_2@C_{60}$. In the most favorable addition products (i.e., addition to bond **1**), the noble gas dimer is totally rotated from the initial position (C_5 axis) to face the attacked C–C bond. However, in some cases the noble-gas dimer is only slightly rotated (bond **3**). As can be seen in Figure 6, at the TS geometry the noble gas dimer has already rotated in both cases (bonds **1** and **3**) to a more favorable situation. Therefore, once 1,3-*cis*-butadiene approaches the fullerene surface to react, the noble gas dimer starts to rotate, either to face the C–C bond that will be attacked (bond **1**) or to a more favorable position (bond **3**). This clearly indicates that as the 1,3-butadiene approaches the fullerene surface, the Ng dimer encapsulated inside rotates (if energetically feasible, vide supra). Moreover, the rotation takes place before the TS is reached.

Interestingly, the lowest activation barrier found for $Xe_2@C_{60}$ is obtained for the addition at [6,6] bond **2** ($\Delta E^{\neq}$ = 3.8 kcal mol^{-1}). The [5,6] bond **e** of the xenon compound undergoes the most exothermic reaction ($\Delta E_R = -45.5$ kcal mol^{-1}) but has a higher activation barrier of 6.1 kcal mol^{-1}. Therefore, for this compound the thermodynamic and the kinetic products do not correspond to the same adduct. However, all bonds that show favorable exothermic reaction energies (**1**, **2**, **a**, **c**, and **e**) have low activation barriers, which range from 3.8 kcal mol^{-1} for bond **2** to 6.1 kcal mol^{-1} for bond **e**. The rest of the considered bonds have significantly higher activation barriers (8.1–16.4 kcal mol^{-1}).

On a whole, a substantial drop in the barrier is found for endohedral fullerenes encapsulating the largest noble gas dimers. The activation barrier for the most favorable addition site decreases along the series $He_2@C_{60} > Ne_2@C_{60} > Ar_2@C_{60} > Kr_2@C_{60} > Xe_2@C_{60}$.

Discussion

The study of the Diels–Alder reaction over the different nonequivalent bonds of the noble gas endohedral fullerenes $Ng_2@C_{60}$ has revealed that the exohedral reactivity of the fullerene is clearly enhanced when noble gas dimers are encapsulated inside, in spite of the following factors that could lead to the opposite conclusion. First, electron transfer takes place from the noble gas to C_{60} (especially in the case of xenon dimer, in which a genuine chemical bond is formed). This electron transfer should in principle decrease the exohedral reactivity, as the electron affinity of the cage is reduced. Second, the C–C distances are in general enlarged on going from $He_2@C_{60}$ to $Xe_2@C_{60}$ (see Table 3), which is usually associated with a decrease in reactivity.[56] Third, it has been observed[19] that $Xe@C_{60}$ is less reactive than $He@C_{60}$, and this has been attributed to the effect of the Xe atom, which pushes the π-electron density of the cage outward and thus hampers the attack of the diene. This last factor, however, is minor according to our calculations showing that the effect of substituting He by Xe in $Ng@C_{60}$ is small, with energy differences of about 0.1 kcal mol^{-1}. Our results for the dimer systems $Ng_2@C_{60}$ show that, whereas the Diels–Alder reaction with $He_2@C_{60}$ and $Ne_2@C_{60}$ is similar to that with free C_{60}, the reaction becomes extremely favorable (additional stabilization of 11–24 kcal mol^{-1}) for argon, krypton, and xenon. This increase in the exohedral reactivity can be understood by considering three factors:

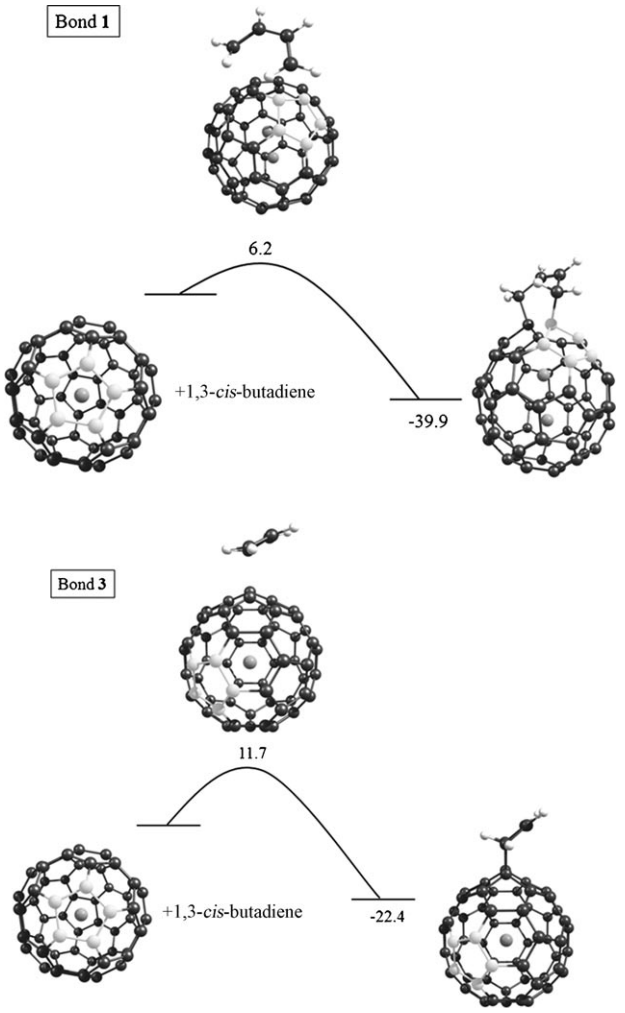

Figure 6. Reaction profile for Diels–Alder reaction at [6,6] bonds **1** and **3** of $Kr_2@C_{60}$. Carbon atoms of the fullerene surface marked in white indicate the initial position of the Ng_2 moiety. At the transition-state geometry, the noble gas dimer has rotated, that is, Ng_2 rotation takes place while 1,3-butadiene approaches the fullerene surface (see text). Energies are given in kcal mol^{-1}.

the molecular orbitals (MOs) of the reactants, the deformation energy of the cage, and the release of compression in the Ng_2 moiety.

Figure 7 shows the MO diagram for all noble gas endohedral fullerenes. The HOMO and LUMO are marked in boldface. The energies and shapes of the MOs are very similar to those reported by Krapp and Frenking for the D_{3d} $Ng_2@C_{60}$ species.[25] The HOMO–LUMO gap of the different endohedral compounds is dramatically different. In the case of $He_2@C_{60}$ the gap is similar to that of free C_{60} (1.63 and 1.66 eV for $He_2@C_{60}$ and free C_{60}, respectively). However, the HOMO–LUMO difference is reduced when larger noble gas dimers are encapsulated: $Ne_2@C_{60}$ (1.57 eV) > $Ar_2@C_{60}$ (1.36 eV) > $Kr_2@C_{60}$ (0.75 eV) > $Xe_2@C_{60}$ (0.18 eV). The reduction in the HOMO–LUMO gap along the He–Xe series is due to a certain stabilization of the LUMO and major destabilization of the HOMO.

The situation for destabilization of the HOMO is complex, because the HOMO of the noble gas endohedral compounds He_2-$Xe_2@C_{60}$ changes along the series. The orbital a_{2u}, which is basically an antibonding (p_z-p_z) σ* orbital in the noble gas dimer (see Figure S5 in the Supporting Information) is the HOMO for $Kr_2@C_{60}$ and $Xe_2@C_{60}$. In contrast, for the lighter homologues this a_{2u} orbital is clearly lower in energy than the a_{1u} orbital, which is the HOMO for $He_2@C_{60}$, $Ne_2@C_{60}$, and $Ar_2@C_{60}$ (see Figure 7). Nevertheless, both the a_{1u} and a_{2u} orbitals are destabilized along the noble gas series. The energy of the orbital a_{1u} changes from −6.23 eV ($He_2@C_{60}$) to −5.93 eV ($Xe_2@C_{60}$), and that of the a_{2u} orbital from −15.76 eV ($He_2@C_{60}$) to −5.07 eV for $Xe_2@C_{60}$ (see Figure 7).

Destabilization of the a_{2u} (p_z-p_z) σ* orbital increases from $He_2@C_{60}$ to $Xe_2@C_{60}$ because of the decreasing Ng–Ng distance along the series. This destabilization of the a_{2u} orbital is also found for free noble gas dimers computed at the geometry they have in the $Ng_2@C_{60}$. This is especially the case for Kr_2 and Xe_2 (the HOMO energy is −8.32 and −5.01 eV for the cases of Xe and Xe_2, respectively, at the BP86/TZVPP level).[25] However, the aforementioned destabilization is enhanced when the dimer is inside the C_{60} cage due to the strong steric repulsion that comes from the Pauli interactions.[25]

The a_{1u} orbital, which is the HOMO for $He_2@C_{60}$, $Ne_2@C_{60}$, and $Ar_2@C_{60}$, shows π-bonding orbital interactions at the [6,6] bonds, and antibonding contributions in the case of [5,6] bonds (see Figure S5, Supporting Information). This is consistent with the usually short [6,6] bond lengths and the long [5,6] bonds (see Table 3). The degenerate e_{1u} orbital is the LUMO for $Xe_2@C_{60}$ but the LUMO+1 for the rest of the endohedral noble gas fullerenes, which instead have an a_{2u} LUMO (see Figure S6 in the Supporting Information). The main interaction between 1,3-*cis*-butadiene and $Ng_2@C_{60}$ occurs between the HOMO of the diene and the LUMO orbitals of the endohedral fullerenes. The higher reactivity found for the [6,6] bonds in the case of the heaviest noble gas atoms can be partially explained by the decrease in LUMO energy along the He–Xe series.

Given the smaller HOMO–LUMO gap found for $Xe_2@C_{60}$, Krapp and Frenking considered the possibility of a triplet electronic ground state instead of a singlet but with a different symmetry (D_{3d}) than we use (D_{5d}).[25] We have also considered this possibility, and the triplet states $(e_{2u})^4(a_{1u})^2(a_{2u})^1(a_{2u})^1(e_{1u})^0$ ("$^3A_{1g}$", the D_{5d} equivalent of the $^3A_{1g}$ state in D_{3d} symmetry) and $(e_{2u})^4(a_{1u})^2(e_{1u})^2(a_{2u})^0(a_{2u})^0$ ("$^3E_{1u}$") were computed by performing a single-point calculation at the optimized geometry of the D_{5d}-$Xe_2@C_{60}$ singlet state. We found energy differences of +3.0 and +24.9 kcal mol^{-1} for $^3A_{1g}$ and $^3E_{1u}$, respectively. Krapp and Frenking found that the most stable configuration for the D_{3d} isomer is the triplet state $^3A_{1g}$, by −3.9 kcal mol^{-1} at the SCS-MP2/TZVPP//BP86/TZVPP level ($^3E_{1u}$ was also more stable than $^1A_{1g}$, by −2.1 kcal mol^{-1}). The correct prediction of spin-state splittings is, however, a widely debated topic, especially for transition metal complexes.[38,57] From these studies, it

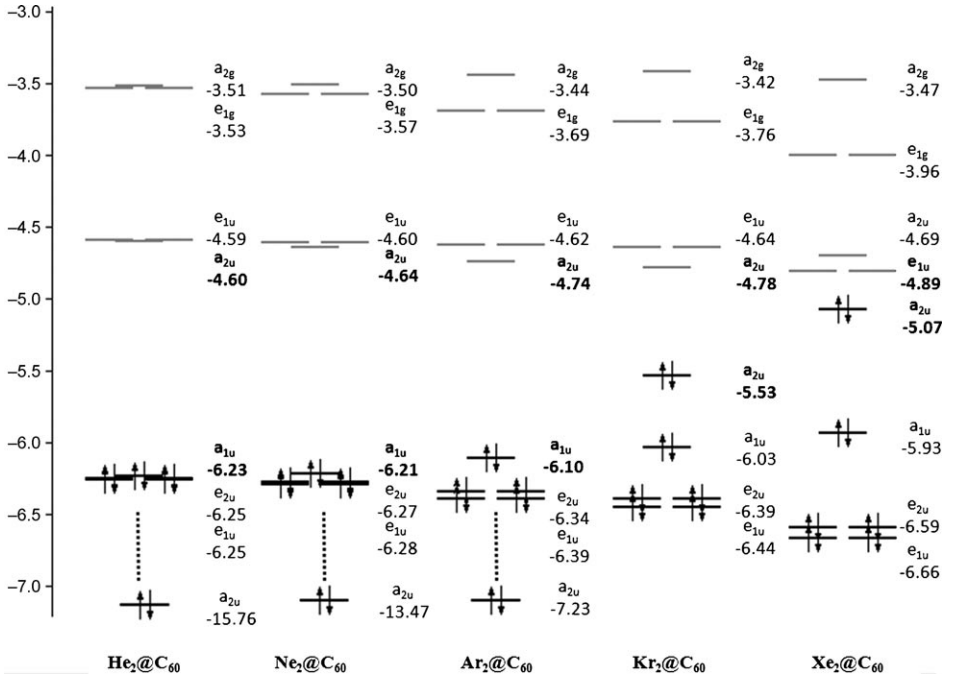

Figure 7. Molecular orbital diagrams for the different endohedral D_{5d}-$Ng_2@C_{60}$ compounds. The HOMOs and LUMOs are marked in boldface. All energies are given in eV.

emerged that reliable spin-state splittings can be obtained by using the OPBE functional[58] in conjunction with STO basis sets.[59] We therefore also performed SP calculations with the OPBE functional, which resulted, like the BP86 functional, in a singlet-spin ground state with the triplet higher in energy by 3.5 kcal mol^{-1}. Therefore, in this study a singlet ground state was considered in all cases for the reactants, transition states, and final products of the xenon endohedral fullerenes.

Obviously, the deformation energy also plays an important role in the high reactivity found for $Xe_2@C_{60}$. The deformation energy of the cage is computed as the difference in energy between free C_{60} and the distorted cage after encapsulation of the noble gas dimers. Insertion of He_2 or Ne_2 inside C_{60} hardly affects the cage, as the deformation energy is approximately 0 kcal mol^{-1} for $He_2@C_{60}$ and less than 1 kcal mol^{-1} for $Ne_2@C_{60}$ (see Table S1, Supporting Information), which concurs with the data obtained by Scuseria and co-workers.[16] These deformation energies are consistent with the reactivities observed, as both the activation barriers and reaction energies of the helium and neon endohedral compounds are very similar to those of free C_{60}. Higher deformation energies are found for the other noble gas dimers: encapsulation of Ar_2, Kr_2, and Xe_2 inside C_{60} leads to deformation energies of 11.2, 22.5, and 34.1 kcal mol^{-1}, respectively. Consistently, longer C–C bonds and highly pyramidalized carbon atoms are observed for these endohedral compounds (see Table 3). This large deformation energy in the case of argon and krypton, and especially for the xenon dimer, also explains partially the high reactivity found for the heavier members of the series. The highly distorted C_{60} cage in $Xe_2@C_{60}$ is extremely reactive and unselective, as the strain of the cage is partially released after reaction.

Finally, we have to consider the release of compression of the Ng_2 unit after cycloaddition. The Ng–Ng distance increases by 0.028, 0.043, 0.040, 0.035, and 0.054 Å when going from the reactant $Ng_2@C_{60}$ to the most stable adduct (product **1**) for He, Ne, Ar, Kr, and Xe, respectively. These increases correspond to stabilization by −0.2, −1.0, −4.1, −5.3, and −10.4 kcal mol^{-1} along the same series (in the case of Xe, we considered the energy difference between free Xe_2^+ at the Xe–Xe distance in optimized $Xe_2@C_{60}$ and in the most stable $Xe_2@C_{60}(C_4H_8)$ adduct). The case of krypton is special, as the total charge in the KrKr moiety at the BP86/TZP level is +0.6 e. Therefore, an intermediate situation between KrKr and $[KrKr]^+$ should be considered (the stabilization is −2.3 and −5.3 kcal mol^{-1} for $[KrKr]^+$ and KrKr, respectively). The energetic stabilization along the series He, Ne, Ar, Kr, and Xe on increasing the Ng–Ng distance from the initial value to that after reaction is higher in the heaviest members of the series. This decompression makes an important contribution to the exothermicity of the reaction in those adducts in which the encapsulated noble gas dimer faces the bond that is being attacked.

Conclusions

The [4+2] Diels–Alder cycloaddition reaction of the noble gas endohedral fullerenes $Ng@C_{60}$ and $Ng_2@C_{60}$ (Ng = He–Xe) with 1,3-*cis*-butadiene has been studied over all nonequivalent bonds of the molecules. In the case of the endohedral compounds encapsulating noble gas dimers, the study was performed from thermodynamic and kinetic points of view. The study on the reactions of $Ng@C_{60}$ compounds showed that the effect of noble gas encapsulation inside the C_{60} cage is not profound, in agreement with experimental results. The obtained reaction energies and activation barriers are close to those of free C_{60}. A slight decrease in exohedral reactivity of the cage occurs on going from He to Ar. However, the reaction energies and activation barriers found for $Xe@C_{60}$ are similar to those obtained for He. More interesting results are obtained for encapsulation of noble gas dimers. The reaction and activation energies indicate that the exohedral reactivity of both $He_2@C_{60}$ and $Ne_2@C_{60}$ are

similar to that of free C_{60}. Like in C_{60}, the most reactive bonds are pyracylenic [6,6] bonds **1** and **2**. For these small elements, rotation of the noble gas dimer is almost barrierless, and during the course of the reaction the Ng_2 moiety rotates to face the attacked bonds. This rotation has little impact on the exohedral reactivity of the cage in the cases of $He_2@C_{60}$ and $Ne_2@C_{60}$.

One might expect reduced exohedral reactivity of endohedral fullerenes encapsulating the heaviest noble gas compared to C_{60} because of electron transfer from the noble gas dimer to the fullerene (especially for the case of Xe_2). This leads to reduced electron affinity of the cage, longer C–C distances, and the π-electron density is pushed outwards from the cage. Nevertheless, the Diels–Alder reaction becomes highly exothermic especially over [6,6] bonds **1** and **2** in $Ar_2@C_{60}$ and $Kr_2@C_{60}$. In these more reactive cases, the noble gas dimer has reoriented to face the attacked bonds. The reactivity of $Xe_2@C_{60}$ is substantially different from those of the rest of the endohedral noble gas compounds, as the reaction becomes extremely exothermic and highly unselective. The Diels–Alder reaction is equally favored over [6,6] and [5,6] bonds situated close to the initial C_5 axis where the noble gas dimer is initially located. Rotation of the heaviest noble gas dimers inside C_{60} is hindered, and bonds close to the C_5 axis are the most reactive, as the noble gas dimer can be reoriented to face the attacked bonds.

The increased reactivity found for the heaviest members of the series is attributed to three factors. First, encapsulation of bigger noble gas atoms such as Kr or Xe inside the cage lowers the LUMO energy. Second, encapsulation of heavy noble gas dimers inside C_{60} leads to highly reactive strained fullerenes. The easiest way to release the strain of the cage is through a reaction which induces pyramidalization of the attacked carbon atoms and breaks the C–C bonds to give a less strained situation. Finally, compression of Ng_2 is released on going from $Ng_2@C_{60}$ to the final adduct.[60]

Acknowledgements

This study was financially supported by the Spanish research projects CTQ2008-03077/BQU and CTQ2008-06532/BQU, the DIUE projects 2009SGR637 and 2009SGR528, and the MICINN fellowship for S.O. no. AP2005-2992. The authors acknowledge the computer resources, technical expertise, and assistance provided by the Barcelona Supercomputing Center - Centro Nacional de Supercomputación.

[1] J. R. Heath, S. C. Obrien, Q. Zhang, Y. Liu, R. F. Curl, H. W. Kroto, F. K. Tittel, R. E. Smalley, *J. Am. Chem. Soc.* **1985**, *107*, 7779–7780; H. W. Kroto, J. R. Heath, S. C. Obrien, R. F. Curl, R. E. Smalley, *Nature* **1985**, *318*, 162–163.

[2] K. A. Caldwell, D. E. Giblin, M. L. Gross, *J. Am. Chem. Soc.* **1992**, *114*, 3743–3756; K. A. Caldwell, D. E. Giblin, C. S. Hsu, D. Cox, M. L. Gross, *J. Am. Chem. Soc.* **1991**, *113*, 8519–8521; T. Weiske, D. K. Böhme, H. Schwarz, *Angew. Chem.* **1991**, *103*, 898–900; *Angew. Chem. Int. Ed. Engl.* **1991**, *30*, 884–886.

[3] M. Saunders, H. A. Jiménez-Vázquez, R. J. Cross, R. J. Poreda, *Science* **1993**, *259*, 1428–1430.

[4] R. J. Cross, A. Khong, M. Saunders, *J. Org. Chem.* **2003**, *68*, 8281–8283.

[5] M. Saunders, R. J. Cross, H. A. Jiménez-Vázquez, R. Shimshi, A. Khong, *Science* **1996**, *271*, 1693–1697; M. Saunders, H. A. Jiménez-Vázquez, R. J. Cross, S. Mroczkowski, M. L. Gross, D. E. Giblin, R. J. Poreda, *J. Am. Chem. Soc.* **1994**, *116*, 2193–2194.

[6] R. L. Murry, G. E. Scuseria, *Science* **1994**, *263*, 791–793.

[7] H. A. Jiménez-Vázquez, R. J. Cross, *J. Chem. Phys.* **1996**, *104*, 5589–5593.

[8] B. A. DiCamillo, R. L. Hettich, G. Guiochon, R. N. Compton, M. Saunders, H. A. Jiménez-Vázquez, A. Khong, J. Cross, *J. Phys. Chem.* **1996**, *100*, 9197–9201; K. Yamamoto, M. Saunders, A. Khong, R. J. Cross, Jr., M. Grayson, M. L. Gross, A. F. Benedetto, R. B. Weisman, *J. Am. Chem. Soc.* **1999**, *121*, 1591–1596.

[9] M. Murata, Y. Murata, K. Komatsu, *Chem. Commun.* **2008**, 6083–6094.

[10] C. M. Stanisky, R. J. Cross, M. Saunders, M. Murata, Y. Murata, K. Komatsu, *J. Am. Chem. Soc.* **2005**, *127*, 299–302; K. E. Whitener, M. Frunzi, S.-i. Iwamatsu, S. Murata, R. J. Cross, M. Saunders, *J. Am. Chem. Soc.* **2008**, *130*, 13996–13999; M. Murata, Y. Murata, K. Komatsu, *J. Am. Chem. Soc.* **2006**, *128*, 8024–8033; S.-i. Iwamatsu, C. M. Stanisky, R. J. Cross, M. Saunders, N. Mizorogi, S. Nagase, S. Murata, *Angew. Chem.* **2006**, *118*, 5463–5466; *Angew. Chem. Int. Ed.* **2006**, *45*, 5337–5340; S.-i. Iwamatsu, T. Uozaki, K. Kobayashi, S. Re, S. Nagase, S. Murata, *J. Am. Chem. Soc.* **2004**, *126*, 2668–2669.

[11] M. Murata, S. Maeda, Y. Morinaka, Y. Murata, K. Komatsu, *J. Am. Chem. Soc.* **2008**, *130*, 15800–15801.

[12] M. Saunders, R. J. Cross, H. A. Jiménez-Vázquez, R. Shimshi, A. Khong, *Science* **1996**, *271*, 1693–1697.

[13] G.-W. Wang, M. Saunders, R. J. Cross, *J. Am. Chem. Soc.* **2001**, *123*, 256–259.

[14] M. Saunders, H. A. Jiménez-Vázquez, R. J. Cross, S. Mroczkowski, D. I. Freedberg, F. A. L. Anet, *Nature* **1994**, *367*, 256–258.

[15] J. Cioslowski, E. D. J. Fleischmann, *J. Chem. Phys.* **1991**, *94*, 3730–3734; M.-S. Son, Y. K. Sung, *Chem. Phys. Lett.* **1995**, *245*, 113–118; M. Bühl, S. Patchkovskii, W. Thiel, *Chem. Phys. Lett.* **1997**, *275*, 14–18; H. Yan, S. Yu, X. Wang, Y. He, W. Huang, M. Yang, *Chem. Phys. Lett.* **2008**, *456*, 223–226; P. Pyykkö, C. Wang, M. Straka, J. Vaara, *Phys. Chem. Chem. Phys.* **2007**, *9*, 2954–2958; V. V. Albert, J. R. Sabin, F. E. Harris, *Int. J. Quantum Chem.* **2007**, *107*, 3061–3066.

[16] R. B. Darzynkiewicz, G. E. Scuseria, *J. Phys. Chem. A* **1997**, *101*, 7141–7144.

[17] L. Becker, R. J. Poreda, T. E. Bunch, *Proc. Natl. Acad. Sci. USA* **2000**, *97*, 2979–2983.

[18] R. Shimshi, A. Khong, H. A. Jiménez-Vázquez, R. J. Cross, M. Saunders, *Tetrahedron* **1996**, *52*, 5143–5148.

[19] M. Frunzi, R. J. Cross, M. Saunders, *J. Am. Chem. Soc.* **2007**, *129*, 13343–13346.

[20] M. Frunzi, H. Xu, R. J. Cross, M. Saunders, *J. Phys. Chem. A* **2009**, *113*, 4996–4999.

[21] D. E. Giblin, M. L. Gross, M. Saunders, H. Jiménez-Vázquez, R. J. Cross, *J. Am. Chem. Soc.* **1997**, *119*, 9883–9890.

[22] A. Khong, H. A. Jiménez-Vázquez, M. Saunders, R. J. Cross, J. Laskin, T. Peres, C. Lifshitz, R. Strongin, A. B. Smith, *J. Am. Chem. Soc.* **1998**, *120*, 6380–6383.

[23] J. Laskin, T. Peres, C. Lifshitz, M. Saunders, R. J. Cross, A. Khong, *Chem. Phys. Lett.* **1998**, *285*, 7–9.

[24] T. Sternfeld, R. E. Hoffman, M. Saunders, R. J. Cross, M. S. Syamala, M. Rabinovitz, *J. Am. Chem. Soc.* **2002**, *124*, 8786–8787.

[25] A. Krapp, G. Frenking, *Chem. Eur. J.* **2007**, *13*, 8256–8270.

[26] T. van der Wijst, C. Fonseca Guerra, M. Swart, F. M. Bickelhaupt, *Chem. Phys. Lett.* **2006**, *426*, 415–421.

[27] T. B. Lee, M. L. McKee, *J. Am. Chem. Soc.* **2008**, *130*, 17610–17619.

[28] N. Martín, *Chem. Commun.* **2006**, 2093–2104; S. Guha, K. Nakamoto, *Coord. Chem. Rev.* **2005**, *249*, 1111–1132.

[29] O. Lukoyanova, C. M. Cardona, J. Rivera, L. Z. Lugo-Morales, C. J. Chancellor, M. M. Olmstead, A. Rodriguez-Fortea, J. M. Poblet, A. L. Balch, L. Echegoyen, *J. Am. Chem. Soc.* **2007**, *129*, 10423–10430; C. M. Cardona, A. Kitaygorodskiy, L. Echegoyen, *J. Am. Chem. Soc.* **2005**, *127*, 10448–10453.

[30] S. Osuna, M. Swart, J. Campanera, J. Poblet, M. Solà, *J. Am. Chem. Soc.* **2008**, *130*, 6206–6214.

[31] S. Osuna, M. Swart, M. Solà, *J. Am. Chem. Soc.* **2009**, *131*, 129–139.

[32] T. Cai, C. Slebodnick, L. Xu, K. Harich, T. E. Glass, C. Chancellor, J. C. Fettinger, M. M. Olmstead, A. L. Balch, H. W. Gibson, H. C. Dorn, *J. Am. Chem. Soc.* **2006**, *128*, 6486–6492; C. M. Cardona, B. Elliott, L. Echegoyen, *J. Am. Chem. Soc.* **2006**, *128*, 6480–6485; L. Echegoyen, C. J. Chancellor, C. M. Cardona, B. Elliott, J. Rivera, M. M. Olmstead, A. L. Balch, *Chem. Commun.* **2006**, 2653–2655; A. Rodríguez-Fortea, J. M. Campanera, C. M. Cardona, L. Echegoyen, J. M. Poblet, *Angew. Chem.* **2006**, *118*, 8356–8360; *Angew. Chem. Int. Ed.* **2006**, *45*, 8176–8180.

[33] ADF2006.01, SCM, E. J. Baerends, J. Autschbach, A. Bérces, F. M. Bickelhaupt, C. Bo, P. L. de Boeij, P. M. Boerrigter, L. Cavallo, D. P. Chong, L. Deng, R. M. Dickson, D. E. Ellis, L. Fan, T. H. Fischer, C. Fonseca Guerra, S. J. A. van Gisbergen, J. A. Groeneveld, O. V. Gritsenko, M. Grüning, F. E. Harris, P. van den Hoek, C. R. Jacob, H. Jacobsen, L. Jensen, G. van Kessel, F. Kootstra, E. van Lenthe, D. A. McCormack, A. Michalak, J. Neugebauer, V. P. Osinga, S. Patchkovskii, P. H. T. Philipsen, D. Post, C. C. Pye, W. Ravenek, P. Ros, P. R. T. Schipper, G. Schreckenbach, J. G. Snijders, M. Solà, M. Swart, D. Swerhone, G. te Velde, P. Vernooijs, L. Versluis, L. Visscher, O. Visser, F. Wang, T. A. Wesolowski, E. van Wezenbeek, G. Wiesenekker, S. K. Wolff, T. K. Woo, A. L. Yakovlev, T. Ziegler, Amsterdam, **2006**.

[34] G. te Velde, F. M. Bickelhaupt, E. J. Baerends, C. Fonseca Guerra, S. J. A. van Gisbergen, J. G. Snijders, T. Ziegler, *J. Comput. Chem.* **2001**, *22*, 931–967.

[35] J. G. Snijders, E. J. Baerends, P. Vernooijs, *At. Nucl. Data Tables* **1981**, *26*, 483–509.

[36] M. Swart, J. G. Snijders, *Theor. Chem. Acc.* **2003**, *110*, 34–41.

[37] E. van Lenthe, E. J. Baerends, J. G. Snijders, *J. Chem. Phys.* **1993**, *99*, 4597–4610.

[38] M. Swart, F. M. Bickelhaupt, *J. Comput. Chem.* **2008**, *29*, 724–734.

[39] S. H. Vosko, L. Wilk, M. Nusair, *Can. J. Phys.* **1980**, *58*, 1200–1211.

[40] A. D. Becke, *Phys. Rev. A* **1988**, *38*, 3098–3100.

[41] J. P. Perdew, *Phys. Rev. B* **1986**, *33*, 8800–8802.

[42] T. P. M. Goumans, A. W. Ehlers, K. Lammertsma, E.-U. Würthwein, S. Grimme, *Chem. Eur. J.* **2004**, *10*, 6468–6475; M. Swart, M. Solà, F. M. Bickelhaupt, *J. Comput. Chem.* **2007**, *28*, 1551–1560.

[43] M. Swart, F. M. Bickelhaupt, *Int. J. Quantum Chem.* **2006**, *106*, 2536–2544.

[44] S. K. Wolff, *Int. J. Quantum Chem.* **2005**, *104*, 645–659.

[45] R. C. Haddon, *J. Phys. Chem. A* **2001**, *105*, 4164–4165; R. C. Haddon, S. Y. Chow, *J. Am. Chem. Soc.* **1998**, *120*, 10494–10496.

[46] R. C. Haddon, QCPE 508/QCMP 044, QCPE Bull. **1988**, 8.

[47] R. Taylor, D. R. Walton, *Nature* **1993**, *363*, 685–693; A. Hirsch, *Angew. Chem.* **1993**, *105*, 1189–1192; *Angew. Chem. Int. Ed. Engl.* **1993**, *32*, 1138–1141; A. Hirsch, *The Chemistry of Fullerenes*, Thieme, Sttutgart, **1994**; W. Śliwa, *Fullerene Sci. Technol.* **1995**, *3*, 243–281; W. Śliwa, *Fullerene Sci. Technol.* **1997**, *5*, 1133–1175.

[48] A. Hirsch, *Top. Curr. Chem.* **1999**, *199*, 1–65.

[49] M. Solà, J. Mestres, J. Martí, M. Duran, *Chem. Phys. Lett.* **1994**, *231*, 325–330; A. Chikama, H. Fueno, H. Fujimoto, *J. Phys. Chem.* **1995**, *99*, 8541–8549.

[50] L. S. K. Pang, M. A. Wilson, *J. Phys. Chem.* **1993**, *97*, 6761–6763.

[51] L. M. Giovane, J. W. Barco, T. Yadav, A. L. Lafleur, J. A. Marr, J. B. Howard, V. M. Rotello, *J. Phys. Chem.* **1993**, *97*, 8560–8561.

[52] M. Straka, J. Vaara, *J. Phys. Chem. A* **2006**, *110*, 12338–12341.

[53] J. M. Campanera, C. Bo, M. M. Olmstead, A. L. Balch, J. M. Poblet, *J. Phys. Chem. A* **2002**, *106*, 12356–12364; J. C. Duchamp, A. Demortier, K. R. Fletcher, D. Dorn, E. B. Iezzi, T. Glass, H. C. Dorn, *Chem. Phys. Lett.* **2003**, *375*, 655–659; Z. Slanina, S. Nagase, *ChemPhysChem* **2005**, *6*, 2060–2063; S. S. Park, D. Liu, F. Hagelberg, *J. Phys. Chem. A* **2005**, *109*, 8865–8873; A. A. Popov, L. Dunsch, *J. Am. Chem. Soc.* **2008**, *130*, 17726–17742.

[54] S. M. Bachrach, P. B. White, *J. Mol. Struct. (THEOCHEM)* **2007**, *819*, 72–78.

[55] G. H. Sarova, M. N. Berberan-Santos, *Chem. Phys. Lett.* **2004**, *397*, 402–407.

[56] M. Solà, J. Mestres, M. Duran, *J. Phys. Chem.* **1995**, *99*, 10752–10758; J. M. Campanera, C. Bo, J. M. Poblet, *J. Org. Chem.* **2006**, *71*, 46–54.

[57] M. Swart, M. Güell, M. Solà in *Accurate Description of Spin States, its Implications for Catalysis* (Ed.: C. F. Matta), Wiley, New York, **2009**, in press.

[58] M. Swart, A. W. Ehlers, K. Lammertsma, *Mol. Phys.* **2004**, *102*, 2467–2474; M. Swart, A. R. Groenhof, A. W. Ehlers, K. Lammertsma, *J. Phys. Chem. A* **2004**, *108*, 5479–5483.

[59] M. Güell, J. M. Luis, M. Solà, M. Swart, *J. Phys. Chem. A* **2008**, *112*, 6384–6391.

[60] **Note added in proof (22.10.2009)**: It has recently been found that the preparation of $He@C_{60}$ and $He_2@C_{60}$ in relatively high efficiency is also achievable using an explosion-based method (see R. F. Peng, S. J. Chu, Y. M. Huang, H. J. Yu, T. S. Wang, B. Jin, Y. B. Fu, C. R. Wang, *J. Mater. Chem.* **2009**, *19*, 3602–3605

Received: May 8, 2009
Published online: October 26, 2009

